Proceedings of the 2016 11th International Pipeline Conference
IPC2016
September 26-30, 2016, Calgary, Alberta, Canada

IPC2016-64549

EFFECT OF COLD-WIRE ADDITION IN THE TSAW PROCESS ON MICROSTRUCTURE AND MECHANICAL PROPERTIES OF THE HAZ OF X70 MICROALLOYED PIPELINE STEEL

Mohsen Mohammadijoo
Department of Chemical and Materials Engineering, University of Alberta, Edmonton, AB, Canada

Stephen Kenny
Research & Development Division, Evraz Inc. NA, P.O. Box 1670 Regina, SK, Canada

Laurie Collins
Evraz Inc. NA, Regina SK, Canada

Hani Henein
University of Alberta, Edmonton AB, Canada

Douglas G. Ivey
University of Alberta, Edmonton AB, Canada

ABSTRACT

Microalloyed steels can achieve a good combination of strength and toughness through appropriate alloy design and thermomechanical controlled processing (TMCP). However, the mechanical properties can deteriorate as a result of the high heat input and thermal cycles that the steel experiences during welding. It is generally accepted that the portion of the heat affected zone (HAZ) adjacent to the fusion line, i.e., the coarse grain heat affected zone (CGHAZ), which is characterized by coarse grains and martensite-austenite (M-A) constituents, is the region with poorer toughness relative to the rest of the steel. In the present research work, modification to the conventional tandem submerged arc welding (TSAW) process is carried out by the addition of a cold wire during welding (CWTSAW), which induces changes to the geometry and properties of the weld joint. Microstructural analysis, mechanical property investigation and geometry analysis indicate overall improvement in the weld and the HAZ properties after cold wire addition. These improvements are explained in terms of an increase in the deposition rate and a decrease in the amount of heat introduced to the weldment. An X70 microalloyed steel was welded using both TSAW and CWTSAW processes. Charpy-V-notch impact testing and microhardness testing showed improvement in the HAZ mechanical properties for CWTSAW samples relative to TSAW samples. Microstructural analysis, using both optical microscopy and scanning electron microscopy (SEM), indicated the formation of finer prior austenite grains (PAG) and less M-A constituent within the CGHAZ of the CWTSAW samples. These improvements are due to lower actual heat introduced to the weldment and a relatively faster cooling rate.

INTRODUCTION

During processing of high strength low-carbon low-alloy steels, a good combination of strength and toughness is obtained by appropriate alloying design and thermomechanical controlled processing (TMCP) [1,2]. However, this strength and toughness combination can be deteriorated by the heat input and the thermal cycles that the steel experiences during welding [3-5]. Since welding is an unavoidable stage in pipe manufacturing, it is essential to produce welded pipe with as low a heat input as possible while retaining adequate joint geometry and properties [4-6]. Submerged arc welding (SAW) has been preferred over other welding process in the pipeline industry due to its inherent properties, such as deep penetration, high deposition rate and capability of welding thick sections [7]. To improve welding productivity in a global economy, many fabricators have resorted to tandem submerged arc welding (TSAW), which is SAW with two to five electrodes [8-10]. Nevertheless, heat input in the TSAW process is increased due to the increase in the overall welding current and voltage needed for a higher deposition rate, resulting in some adverse effects on the microstructure and toughness of the weld joint. It is generally accepted that the portion of the base metal which is affected by the heat of welding, the heat affected zone (HAZ), and particularly the zone adjacent to the fusion line, the coarse grain heat affected zone (CGHAZ), has lower toughness relative to the rest of the steel. The deterioration in toughness in the CGHAZ is attributed to the formation of large prior

austenite grains (PAG) and martensite-austenite (M-A) constituents, which are localized brittle zones (LBZ), as a result of the high peak temperature and relatively fast cooling rate in the CGHAZ [3,4,11-13].

In the present research work, cold-wire TSAW (CWTSAW) is developed to improve the microstructure and the mechanical properties of the HAZ, while maintaining appropriate weld geometry. The process involves two electrodes with arcs and one electrically cold electrode. In CWTSAW, the additional cold wire can be fed into the tandem weld pool, resulting in a higher deposition rate and better productivity for the welding process without increasing heat input compared with the TSAW process [14-16]. Furthermore, incorporating a cold wire in TSAW moderates the heat input by consuming the heat energy of the trail electrode, leading to a lower amount of heat introduced to the weldment. Accordingly, better quality welds are expected at lower heat inputs per mass of deposited material and with a substantial reduction in arcing time leading to the formation of a smaller and shorter weld pool (compared with TSAW without a cold wire). As such, CWTSAW technology is a promising technique for pipe seam welds commonly used in the pipeline industry. The results of the present research work show that the reduction in the overall heat input by cold wire addition causes some improvement in microstructure and, consequently, properties of the HAZ. Full metallographic examinations are carried out using optical microscopy and scanning electron microscopy (SEM). Charpy-V-notch impact testing and microhardness testing are performed to investigate and correlate the properties changes with microstructure alterations in the HAZ of samples prepared by CWTSAW.

MATERIALS & EXPERIMENTAL PROCEDURE

X70 microalloyed steel plates, 12.4 mm in thickness and fabricated by Evraz Inc. NA, were used as the base metal. The weld samples were prepared by both CWTSAW and TSAW processes using two 4 mm diameter EA2 electrodes (according to the ASME standard) and one cold wire with the same diameter and composition as the electrodes. The flux was chosen according to EN 760 (BF6.5, Bavaria, Germany). The chemical compositions of the microalloyed steel and consumable electrode are indicated in Table 1.

Table 1. X70 steel and electrode compositions (key alloying elements)

X70 composition (wt%)							
C	**S**	**Mn**	**N**	**Ni**	**Nb**	**Ti**	**Pcm**
0.04	0.001	1.76	0.0098	0.1	0.078	0.017	0.175
Electrode and cold wire composition (wt%)							
BA-	**C**	**Mn**	**Mo**	**Cu**	**Cr**	**Si**	**Ni**
S2Mo	0.1	1.04	0.56	0.03	0.03	0.1	0.02

A 90° V-shaped bevel, 5 mm in depth, was machined in the steel plates prior to welding. Direct current electrode positive (DCEP) and square wave alternating current (ACSQ) polarity were employed, using constant current type power sources to operate the lead and trail electrodes, respectively. In previous papers [17,18], the CWTSAW process parameters were investigated and optimized in terms of geometry, dilution and microhardness of the weld and the HAZ. The present CWTSAW process setup has been developed based on the optimized welding parameters. More details of the welding procedure have been discussed elsewhere [17,18]. The welding conditions to fabricate the microalloyed steel joint are presented in Table 2. The fabricated welds were visually inspected prior to any further investigation to ensure that the welds were free from the macro-level defects, such as surface porosity, hot-cracking, undercutting and burn-through. Figure 1 depicts the steel plate geometry and the CWTSAW process setup employed to fabricate weld samples. The heat input for both welding processes was constant and set at 22.2 kJ/cm. All welding parameters were the same for both processes other than the additional cold wire to investigate the effect of cold wire addition on microstructure and mechanical properties of the HAZ.

Table 2. Welding process parameters

Process Parameter	Unit	CWTSAW	TSAW
Current- Lead Electrode	A	1040	1040
Current- Trail Electrode	A	830	830
Voltage- Lead Electrode	V	30	30
Voltage- Trail Electrode	V	34	34
Welding Travel Speed	mm/s (in/min)	26.67 (63)	26.67 (63)
Cold Wire Position	--	Lagging	NA
Cold Wire Angle	°	63	NA
Cold Wire Feed Speed	mm/s (in/min)	4.23 (10)	NA

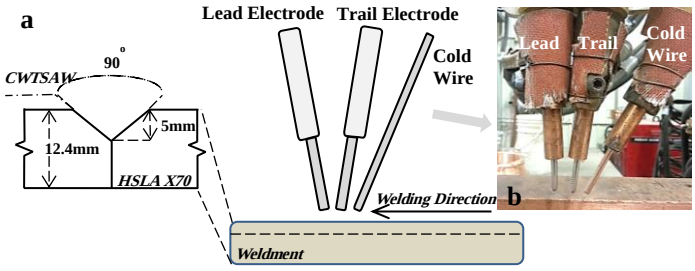

Figure 1. CWTSAW process setup. (a) Schematic view of joint configuration along with the positioning of the electrodes and cold wire and (b) welding setup designed at Evraz Inc. NA

Charpy impact tests were performed on subsize Charpy-V-notch (CVN) bars, 5 mm x 10 mm x 55 mm in size, at room temperature (RT) and -30°C. The Charpy specimens were machined in the transverse orientation relative to the welding direction according to ASTM E23-12c [19]. Due to the bulbous shape of the weld metal (WM) and the HAZ and the small size of the HAZ, it was not possible to fabricate full size Charpy specimens of the HAZ. As such, subsize specimens were extracted as close to the top metal surface as possible to ensure that half of the notch was located in the CGHAZ and half was

located in the fine grain heat affected zone (FGHAZ). Figure 2(a) illustrates the location of the notch for the toughness investigation. two transverse samples of each weld were mounted, ground and polished according to the ASTM E3-11 standard [20] for microhardness analysis (ASTM E384 [21]). Both CVN and microhardness samples were then etched with 4% Nital to reveal the boundary between different zones of the steel weld. A 500 g load was applied for a dwell time of 14 s per indentation. In total, 20 test points were examined per weld sample, with an average of 7-9 indents across each of the FGHAZ and CGHAZ. Three sets of indentations were used for each weld at different locations to increase the number of the data sets. Figure 2(b) depicts the hardness measurement mapping for a typical welded sample using CWTSAW.

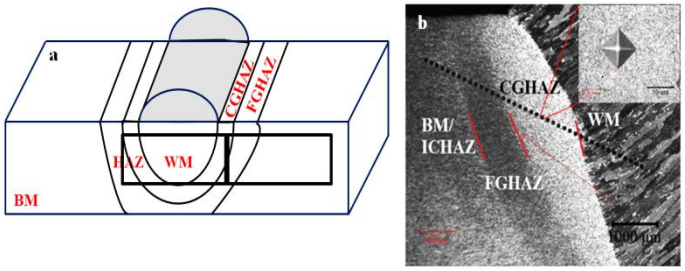

Figure 2. (a) Schematic view of extraction of CVN specimen from the weld sample. (b) Microhardness mapping along the BM, HAZ and WM of a typical weld prepared by CWTSAW. The micrograph in the inset shows an indentation in the CGHAZ

Microstructural analysis was carried out on weld samples using optical microscopy (Olympus BX61) and scanning electron microscopy (Tescan Vega-3 SEM). The formation and fraction of M-A constituents is dependent on the cooling rate and the prior austenite grain (PAG) size [12,13,22]. Revealing PAG boundaries and M-A constituents in microalloyed steels and their relevant welds can be difficult to achieve and depends very much on the etchant type and time. As such, several etching procedures, using various etchants with different solution concentrations and etching times, were employed. After the etching trials, a chemical solution containing 4 g of picric acid in 96 ml ethanol along with a few drops of HCl acid was selected to clearly reveal the PAG boundaries. The PAG size was analyzed using the mean lineal intercept method according to ASTM E112 [23]. Freshly polished specimens were then color etched through a separate process using LePera's etchant for 30-50 s to reveal different microstructural features. Microstructural analysis indicated a high sensitivity of phase identification to etchant composition and etching time. Quantitative analysis of the M-A constituent was done using ImageJ commercial image analysis software. The fraction of other microstructure features was examined according to ASTM E562 standard [24]. Fractography of the CVN specimens was performed by SEM.

RESULTS & DISCUSSION

Impact Toughness:

The HAZ Charpy impact toughness results at two different temperatures for samples welded by CWTSAW and TSAW are presented in Fig. 3. The average of nine Charpy tests and the minimum impact energy for each weld are presented. The minimum Charpy absorbed energy represents the lowest toughness that was measured and may be important from an engineering perspective. According to Fig. 3, there is a slight increase in the impact energy (both the average and minimum values) through the addition of a cold wire to the conventional TSAW process, with a corresponding reduction in the actual heat introduced to the weldment. The large error bars for the HAZ weld samples at -30°C are most likely due to the ductile-to-brittle transition temperature (DBTT) for this steel, which is close to -30°C. In this regard, Graham [25] reported that the Charpy absorbed energy data for ferritic steels commonly exhibits large scatter in the DBTT region. Additional Charpy tests will be done at lower temperatures to determine the DBTT for both welding processes. Since toughness is influenced by a number of microstructural factors, such as grain size, matrix microstructure and the shape, size and distribution of M-A constituents, microstructural alterations within the HAZ are evaluated and discussed below.

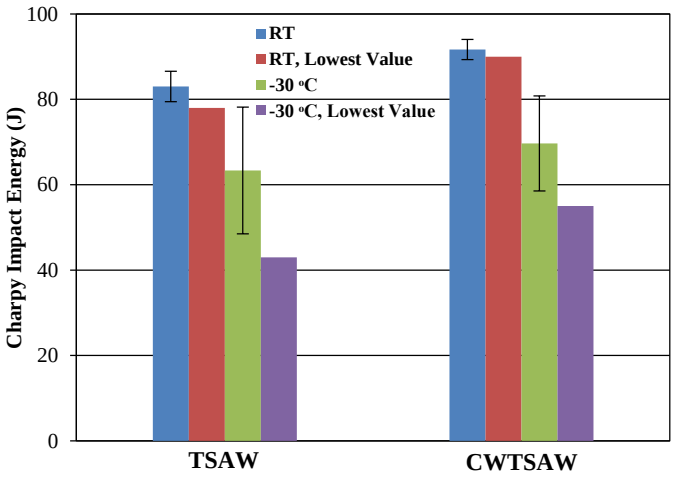

Figure 3. Charpy impact toughness of the HAZ for steel samples welded by CWTSAW and TSAW processes (error bars: the standard deviation)

Microhardness:

In addition to the Charpy impact testing, the weld samples fabricated using the CWTSAW and TSAW processes were evaluated in terms of HAZ geometry and microhardness. In the CWTSAW process, the resultant CGHAZ area was narrower compared with the CGHAZ area for the TSAW process due to lower actual heat introduced to the weldment by cold wire addition and corresponding faster cooling rate [17,18]. Figure 4 depicts macrographs of two weld samples prepared via the CWTSAW and TSAW processes. The results of four geometry measurements of the fabricated welds indicated that there was a

reduction from 21.56±0.63 mm^2 to 20.03±0.50 mm^2 in the CGHAZ area. However, the influence of cold wire addition on the dilution and geometry of the weld and HAZ is increased by increasing the feeding speed of the cold wire, which has been discussed in detail elsewhere [17]. The weld deposition rate was increased by 6%, when the cold wire was fed at a rate of 4.23 mm/s (10 in/min).

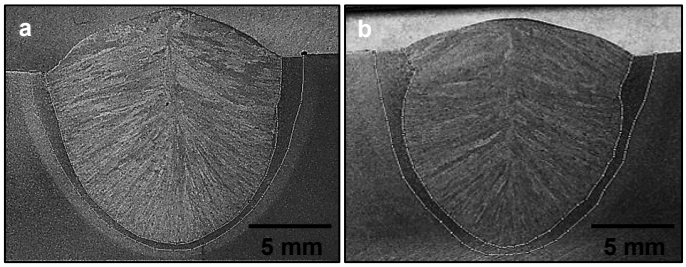

Figure 4. Macrographs of welds produced by: (a) CWTSAW and (b) TSAW. The CGHAZ is outlined in both images

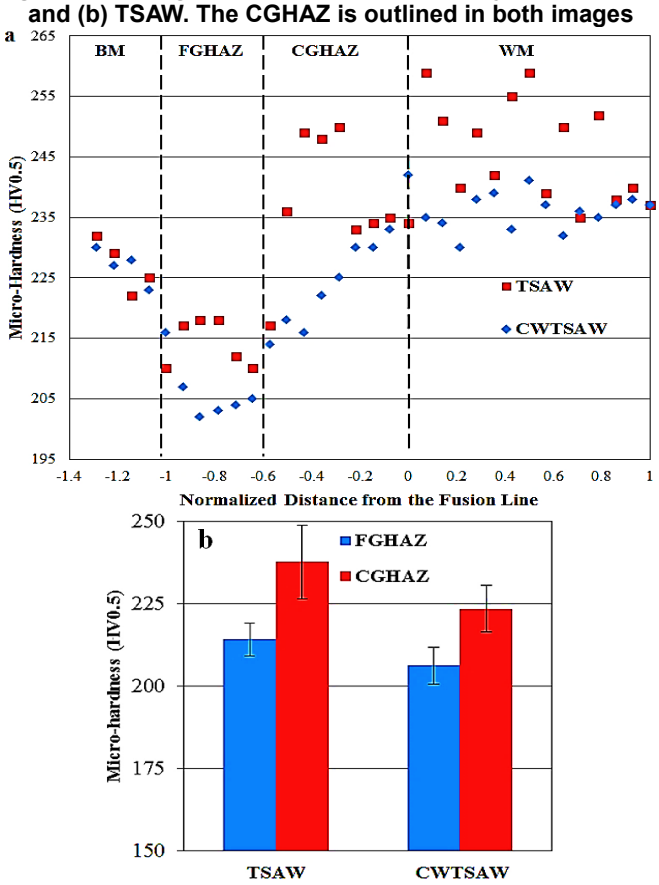

Figure 5. (a) Microhardness variation within the weld samples. (b) Average microhardness with the standard deviation for the FGHAZ and CGHAZ of the steel samples welded by the CWTSAW and TSAW processes

Figure 5 depicts the microhardness variations along the HAZ and the WM. The microhardness value of the as-received base metal (BM) was measured as 228±4 HV. As shown in Fig. 5, the microhardness of the CGHAZ was reduced by the addition of a cold wire to the TSAW process. It is generally agreed [11-13] that the CGHAZ of welded microalloyed steels, which is characterized by a coarse grained microstructure and M-A constituents (LBZ), is the region in the steel with unfavorable fracture toughness compared with the rest of the steel. The CWTSAW sample showed a reduction in the size of CGHAZ and a reduction in the CGHAZ microhardness, due to a reduction in the actual heat introduced to the weldment and the corresponding microstructural changes. The lower fraction of M-A constituents (LBZ) formed within the HAZ resulted in lowering of the microhardness in the HAZ. The microstructural alterations within the HAZ are discussed in the following subsection.

Microstructure:

The microstructure for the X70 microalloyed steel was a combination of 86.9% polygonal ferrite, 9.2% granular bainite, 3.0% bainitic ferrite and a fine distribution of 0.9% M-A constituents; the PAG size was ~8 µm. The PAG size and the fraction, size and shape of the microstructural features are altered in the HAZ due to the heat input and thermal cycle that the steel experiences during welding [26]. Refining the PAG size influences the transformation products, particularly the M-A constituents, within the HAZ, which results in beneficial effects on toughness [12,13,22]. However, there has only been limited work done to correlate the PAG size and M-A constituents [12,13,22]. Optical micrographs of the HAZ, revealing the PAGs and M-A constituents are shown in Figure 6(a)-(f). The PAG size in the CGHAZ (Fig. 6(a)-(b)) and the FGHAZ was decreased by addition of the cold wire. The PAG size in the CGHAZ and FGHAZ for TSAW and CWTSAW samples was measured as 68 µm and 5.5 µm, and 55 µm and 4.7 µm, respectively. The reduction in the PAG size in the CGHAZ is attributed to a reduction in the actual heat introduced to the weldment, lowering of the peak temperature, reduction in the retention time in the austenitization temperature range (1100-1400°C) and an increase in the cooling rate by adding the cold wire. The M-A constituents along with other microstructural features in the CGHAZ and FGHAZ of the two samples are shown in Fig. 6(c)-(f). The M-A constituents are revealed as white regions using LePera's etchant [27]. SEM micrographs of the CGHAZ of the weld samples are depicted in Fig. 7(a)-(b). The CGHAZ microstructure of the TSAW sample (with higher heat input) has large PAGs, polygonal ferrite (PF), granular bainite (GB), bainitic ferrite (BF) and large M-A constituents, which are mostly formed along the PAG boundaries. In contrast with the TSAW sample, the CGHAZ microstructure of the CWTSAW sample (with lower heat input) is composed of finer PAGs, PF, GB and BF associated with fine, blocky shaped M-A constituents. However, less M-A is formed along the CGHAZ of the CWTSAW weld sample compared with the TSAW sample. The microstructure of the FGHAZ of the CWTSAW sample is composed of PF and less GB and BF with smaller M-A constituents compared with the FGHAZ of the TSAW sample. Phase fraction analysis of the transformation products in the CGHAZ and FGHAZ of the welded samples is indicated in Fig. 8.

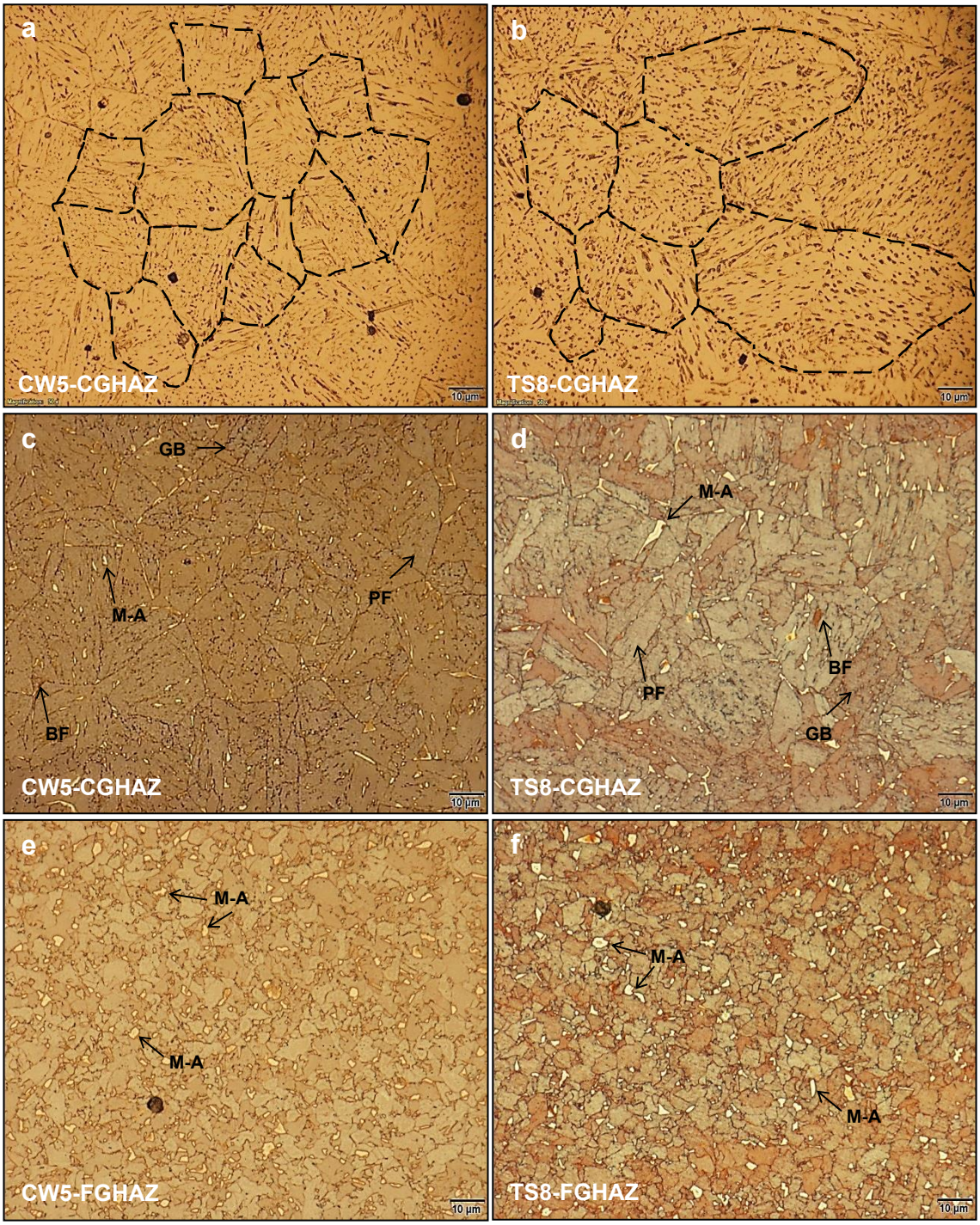

Figure 6. Optical micrographs of the CGHAZ and FGHAZ for the CWTSAW (CW5) sample (a,c,e) and the TSAW (TS8) sample (b,d,f). Images (a-d) and (e-f) are from the CGHAZ and FGHAZ, respectively

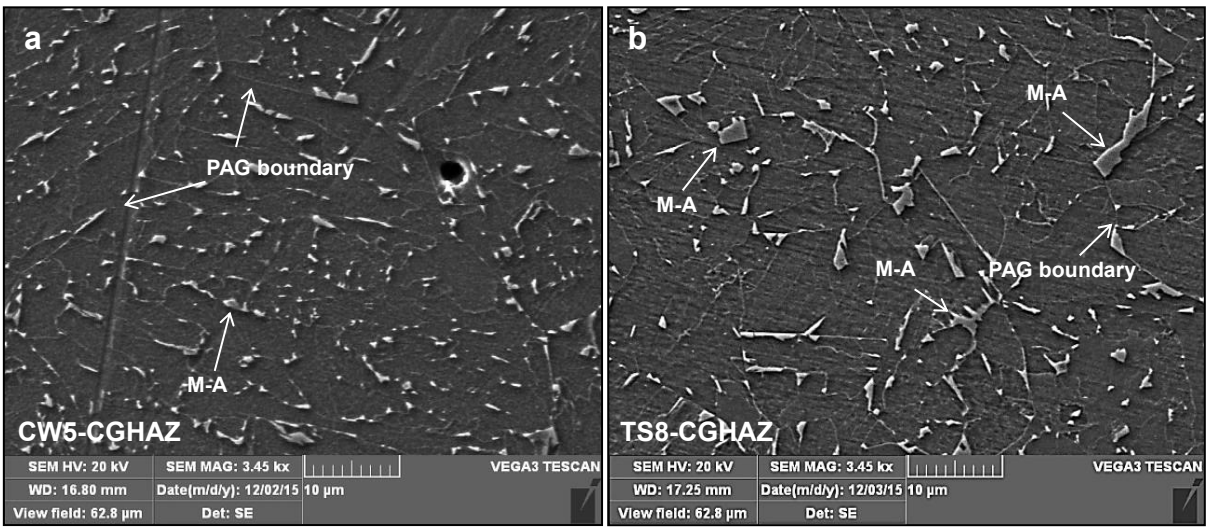

Figure 7. SEM secondary electron (SE) images of the CGHAZ. (a) the CWTSAW (CW5) sample and (b) the TSAW (TS8) sample

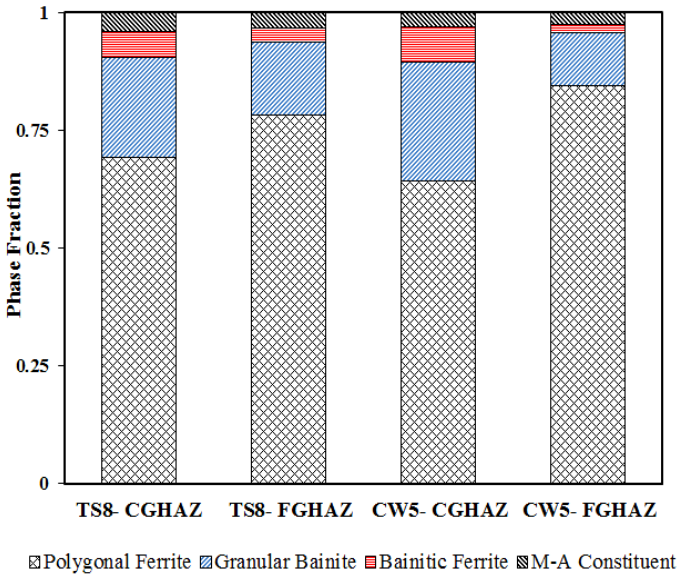

Figure 8. Microstructural constituent analysis in the FGHAZ and CGHAZ for the microalloyed steel welded by the CWTSAW (CW5) and TSAW (TS8) processes

The M-A fraction in the CGHAZ, determined from the optical micrographs, was 4.1% and 3.0% for the TSAW and CWTSAW samples, respectively, indicating a reduction in the fraction of M-A as a consequence of PAG size reduction [11,12] by cold wire addition. The M-A fraction in the CGHAZ of TSAW and CWTSAW samples, calculated from the SEM micrographs, was 5.4% and 3.3%, respectively. The trend is the same and the actual values are quite similar for both techniques, which confirms the validity of the M-A identification in the optical images. The M-A fraction in the FGHAZ of the TSAW and CWTSAW samples was 3.6% and 2.7%, respectively. Quantitative analysis of the M-A regions indicates that the fraction of M-A constituents in the CGHAZ with the size larger than 2 µm for TSAW and CWTSAW samples is 3.5% and 0.9%, respectively. The low toughness in the CGHAZ of welded microalloyed steels is highly influenced by the shape, size, distribution and fraction of M-A constituents in the CGHAZ [11,12]. The larger M-A constituents in the CGHAZ of the TSAW sample are due to the higher martensite start temperature (Ms) for samples with larger PAGs [12,28-30]. Bhadeshia et al. [28,29], Heinze et al. [31] and Guimaraes [32] suggested that a decrease in Ms temperature happens with a decrease in the PAG size, which results in a lower volume fraction of martensite. According to the classical Koistinen-Marburger (KM) equation [33] and the geometrical partitioning model by Fisher et al. [34], the fraction of martensite is a function of the amount of undercooling below the Ms temperature. Based on the proposed models, the martensite volume fraction formed in the early stages of the transformation is proportional to the PAG size cubed; hence, "the fraction of the transformation needed to detect Ms is reached at a smaller undercooling when the PAG size is larger" [28]. Therefore, a coarser PAG size increases the fraction and size of the M-A constituent. Yu et al. [11] and Li et al. [12] showed that a coarse PAG size, associated with a coarse M-A constituent, is the dominant factor in promoting brittle fracture in the CGHAZ. Accordingly, there is a concurrent effect of both grain size refinement and M-A transformation, which plays a significant role in the strength and toughness of the HAZ. Due to the formation of the M-A constituent, there is a higher proportion of LBZs in the CGHAZ of the TSAW sample compared with the CWTSAW sample. This shows up as higher microhardness values in the CGHAZ for the TSAW sample relative to the CWTSAW sample. Also, a narrower distribution of fine M-A constituents (LBZs) inside the ferritic matrix in the CGHAZ of the CWTSAW sample resulted in a slightly higher fracture toughness for the HAZ. However, coarser PAGs with large M-A constituents, which are mostly formed along the PAG

boundaries, lead to inferior toughness properties in the HAZ of the TSAW sample. This inferior toughness, due to formation of M-A constituents along PAG boundaries, is confirmed by the research work done by Davis et al. [35,36] and Reichert et al. [37]. They found that the combination of an elongated shape and the formation of a network of M-A constituents along the PAG boundaries is most detrimental to fracture properties. The improved microstructural alterations and consequent mechanical property changes in the HAZ of the CWTSAW sample are attributed to the lower actual heat introduced to the steel and the lower peak temperature along the HAZ by the addition of the cold wire during welding.

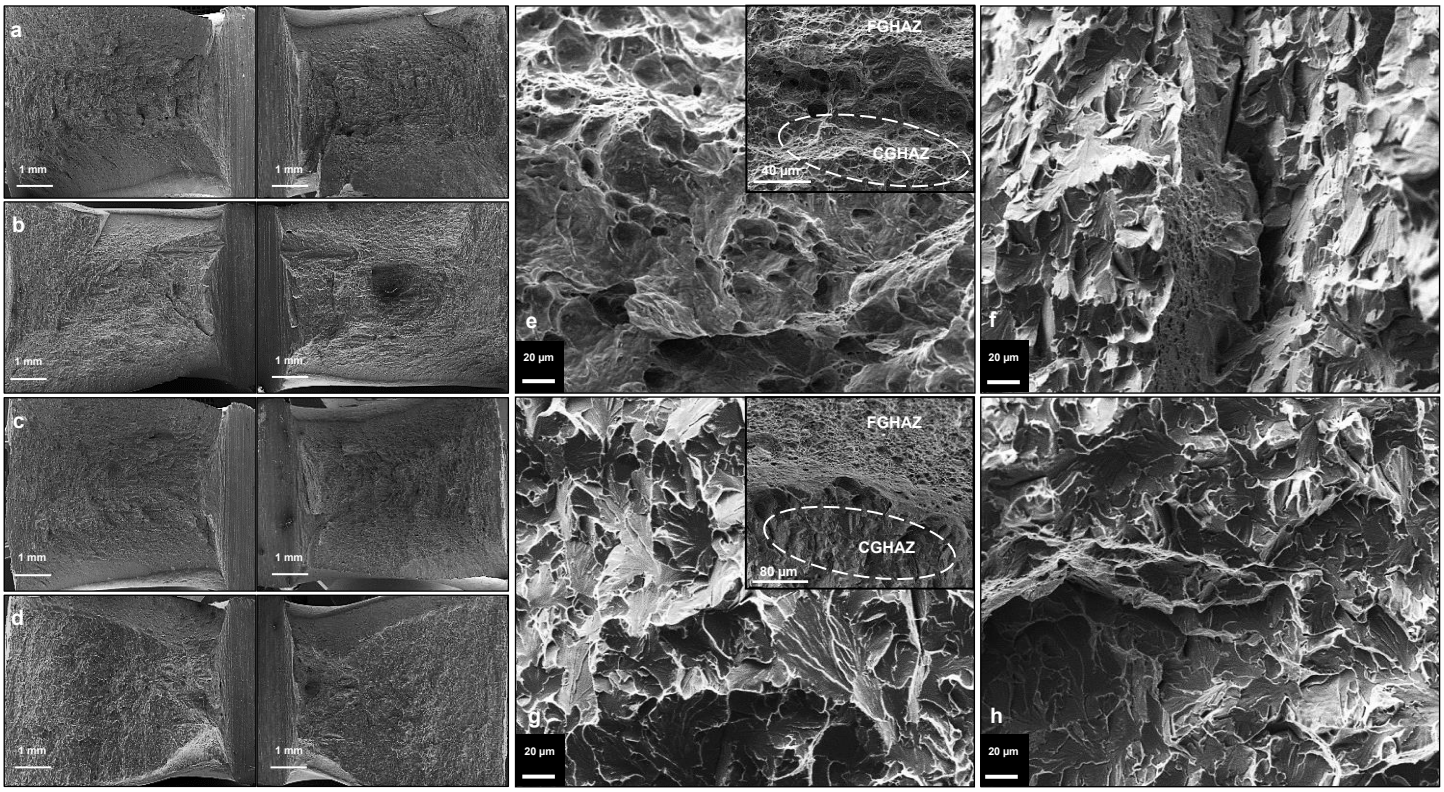

Figure 9. SEM SE fractographs of specimens welded by (a,b) CWTSAW and (c,d) TSAW processes. Micrographs showing the fracture surfaces in the CGHAZ of specimens welded by (e,f) CWTSAW and (g,h) TSAW. The insets in (e) and (g) show the boundary between FGHAZ and CGHAZ in the weld specimens. Micrographs (a,c,e,g) and (b,d,f,h) are at RT and -30°C, respectively.

Fracture Analysis:

According to the impact toughness results shown in Fig. 3, the HAZ toughness of the TSAW sample is lower compared with the CWTSAW sample. As stated in the previous subsection, this reduction in toughness of the HAZ of the TSAW sample is attributed to the formation of large M-A constituents inside and along the PAG boundaries as a result of the higher actual heat input. Lowering the heat input by adding the cold wire altered the size, shape, distribution and fraction of the M-A constituent, leading to an improvement in the HAZ toughness. The reduction in toughness by increasing welding heat input has been confirmed in the literature [6,26,38]. The fracture surface morphologies of the HAZ at two different test temperatures for the CWTSAW and TSAW samples are illustrated in Fig. 9(a,b,e,f) and 9(c,d,g,h), respectively. The boundary between the CGHAZ and FGHAZ on the fracture surface is shown in the inset micrographs in Fig. 9(e,g). The fracture in the FGHAZ and CGHAZ of the CWTSAW weld sample (at RT) is fully ductile and the fracture mechanism involves microvoid coalescence (MVC). However, the fracture mechanism in the FGHAZ and CGHAZ for the TSAW weld sample at RT is different, i.e., MVC and quasi-cleavage, respectively, resulting in ductile and quasi-brittle fracture in the FGHAZ and CGHAZ at RT. Due to the large PAG size in the CGHAZ of the TSAW sample, large cleavage facets are present on the fracture surface, which contribute to lowering of the Charpy energy in the HAZ of the TSAW sample. A combination of MVC and quasi-cleavage, along with intergranular fracture, is seen on the CGHAZ fracture surface of the CWTSAW sample at -30°C. However, the CGHAZ fracture surface of the TSAW sample consists of a mixture of cleavage and intergranular facets, resulting in brittle fracture in the CGHAZ of the TSAW sample at -30°C [39]. The M-A constituent is significantly harder than the internal grain microstructure, so that cracks initiate easily between two closely spaced large M-A constituents. Moeinifar et al. [8]

concluded from their microstructural study of multiple TSAW samples that the size and shape of M-A constituents are significant factors affecting the Charpy impact properties of the CGHAZ and that microcrack nucleation may occur from M-A islands at the intersection of PAG boundaries. Moreover, Li et al. [40] found that an intercritically reheated CGHAZ demonstrated the lowest toughness, due to the presence of M-A constituents with high carbon content martensite. The large slender shaped M-A constituents in the CGHAZ of the TSAW sample of this work formed mostly along the PAG boundaries and can promote the formation of microcracks, resulting in brittle/quasi-brittle fracture in the HAZ.

CONCLUSIONS

Tandem submerged arc welding (TSAW) with an additional cold wire (CWTSAW) has been compared with TSAW in terms of heat affected zone (HAZ) microstructure, mechanical properties and geometry. Microstructural evolution and its influence on the fracture toughness of the weld HAZ by cold wire addition in the TSAW process has been studied for the first time through this research work. Cold wire addition resulted in a reduction in the prior austenite grain (PAG) size in the coarse grained HAZ (CGHAZ). Microstructural analysis showed that the fraction and size of M-A constituents in the CGHAZ were reduced, and the distribution and shape were altered, when a cold wire was added to the TSAW process. The changes to the fraction and characteristics of the M-A constituents in the HAZ are attributed to the lower actual heat introduced to the weldment, the lower peak temperature and the formation of finer PAGs by cold wire addition. The relatively large elongated M-A constituents which mostly form along the PAG boundaries, along with the relatively large PAGs, of the TSAW samples (compared with those of the CWTSAW) led to inferior toughness properties in the HAZ of the TSAW sample, since the larger M-A constituents can stimulate the formation of microcracks leading to intergranular fracture.

ACKNOWLEDGEMENTS

The present study is financially supported by the Natural Sciences and Engineering Research Council (NSERC) of Canada, Evraz Inc. NA, TransCanada PipeLines Ltd., Enbridge Pipelines Inc., UT quality Inc. and Alliance Pipeline Ltd. Special thanks go to the Research and Development Division of Evraz Inc. NA for providing equipment and technical assistance to conduct the welding runs and Charpy testing.

REFERENCES

[1] Shukla, R., Ghosh, S. K., Chakrabarti, D., and Chatterjee, S., 2013, "Microstructure, Texture, Property Relationship in Thermo-Mechanically Processed Ultra-Low Carbon Microalloyed Steel for Pipeline Application," *Materials Science & Engineering A., Vol. 587*, pp. 201-208.

[2] Ming-Chun, Z., Yang, K., and Shan, Y., 2002, "The Effects of Thermo-Mechanical Control Process on Microstructures and Mechanical Properties of a Commercial Pipeline Steel," *Materials Science & Engineering A., Vol. 335*, pp. 14-20.

[3] Ying-Qiao, Z., Han-Qian, Z., Jin-Fu, L., and Wei-Ming, L., 2009, "Effect of Heat Input on Microstructure and Toughness of Coarse Grain Heat Affected Zone in Nb Microalloyed HSLA Steels," *Journal of Iron Steel Research International, Vol. 16*, pp. 73-80.

[4] Xia, Z. H., Wan, X. L., Tao, X. L., and Wu, K. M., 2012, "Effect of Heat Input on Toughness of Coarse-grained Heat-affected Zone of an Ultra-Low Carbon Acicular Ferrite Steel," *Advanced Materials Research, Vol. 538*, pp. 2003-2008.

[5] Wan, X. L., Wang, H. H., Cheng, L., and Wu, K.M., 2012, "The Formation Mechanisms of Interlocked Microstructures in Low-Carbon High-Strength Steel Weld Metals," *Materials Characterization, Vol. 67*, pp. 41-51.

[6] Liang, G. L., Yang, S. W., Wu, H. B., and Liu, X. L., 2013, "Microstructure and Mechanical Performances of CGHAZ for Oil Tank Steel during High Heat Input Welding," *Rare Metals, Vol. 32*, pp. 129-133.

[7] Qiao, G. Y., Xiao, F. Y., Zhang, X. B., Cao, Y. B., and Liao, B., 2009, "Effects of Contents of Nb and C on Hot Deformation Behaviors of High Nb X80 Pipeline Steels," *Transactions Nonferrous Metals Society of China, Vol. 6*, pp. 1395-1399.

[8] Moeinifar, S., Kokabi, A. H., & Madaah Hosseini, H. R., 2011, "Role of Tandem Submerged Arc Welding Thermal Cycles on Properties of the Heat Affected Zone in X80 Microalloyed Pipe Line Steel," *Journal of Materials Processing Technology, Vol. 211*, pp. 368-375.

[9] Kiran, D., Alam, S., and De, A., 2013, "Development of Process Maps in Two-Wire Tandem Submerged Arc Welding Process of HSLA Steel," *Journal of Materials Engineering Performance, Vol. 22*, pp. 988-994.

[10] ESAB, 2014, "Submerged arc welding technical handbook," ESAB publishing.

[11] Yu, L., Wang, H. H., Hou, T. P., Wang, X. L., Wan, X. L., and Wu, K. M., 2014, "Characteristic of Martensite-Austenite Constituents in Coarse Grained Heat Affected Zone of HSLA Steel with Varying Al Contents," *Science and Technology of Welding and Joining, Vol. 19*, pp. 708-714.

[12] Li, X., Ma, X., Subramanian, S. V., Shang, Ch., and Misra, R. D. K., 2014, "Influence of Prior Austenite Grain Size on Martensite-Austenite Constituent and Toughness in the Heat Affected Zone of 700 MPa High Strength Linepipe Steel," *Materials Science & Engineering A., Vol. 616*, pp. 141-147.

[13] Li, X., Fan, Y., Ma, X., Subramanian, S. V., and Shang, C., 2015, "Influence of Martensite-Austenite Constituents Formed at Different Intercritical Temperatures on Toughness," *Materials Design, Vol. 67*, pp. 457-463.

[14] Mruczek, M. F., 2006, "Cold Wire Feed Submerged Arc Welding," Technical report, Advanced Technology Institute, SC.

[15] Ramakrishnan, M., and Muthupandi, V., 2013, "Application of Submerged Arc Welding Technology with Cold Wire Addition for Drum Shell Long Seam Butt Welds of Pressure Vessel Components," *International Journal of Advanced Manufacturing Technology, Vol. 65*, pp. 945-956.

[16] Ramakrishnan, M., Padmanaban, K., and Muthupandi, V., 2013, "Studies on Fracture Toughness of Cold Wire Addition in Narrow Groove Submerged Arc Welding Process," *International*

Journal of Advanced Manufacturing Technology, Vol. 68, pp. 293-316.
[17] Mohammadijoo, M., Kenny, S., Wiskel, J. B., Henein, H., and Ivey, D. G., 2015, "Cold-wire Tandem Submerged Arc Welding: A Novel Technique for Pipeline Manufacturing," *Proceedings, 54th Conference of Metallurgists*, Toronto, ON.
[18] Mohammadijoo, M., Kenny, S., Collins, L., Henein, H., and Ivey, D. G., 2016, "Influence of Cold-Wire Tandem Submerged Arc Welding Parameters on Weld Geometry and Microhardness of Microalloyed Pipeline Steels," *International Journal of Advanced Manufacturing Technology,* In Press.
[19] ASTM E23-12c, 2012, "Standard Test Methods for Notched Bar Impact Testing of Metallic Materials," ASTM International, PA.
[20] ASTM E3-11, 2011, "Standard guide for preparation of metallographic specimens," ASTM International, PA.
[21] ASTM E384, 2012, "Standard Test Method for Knoop and Vickers Hardness of Materials," ASTM International, PA.
[22] Prawoto, Y., Jasmawati, N., and Sumeru, K., 2012, "Effect of Prior Austenite Grain Size on the Morphology and Mechanical Properties of Martensite in Medium Carbon Steel," *Journal of Materials Science and Technology, Vol. 28*, pp. 461-466.
[23] ASTM E112, 2012, "Standard Test Method for Determining Average Grain Size," ASTM International, PA.
[24] ASTM E562, 2011, "Standard Test Method for Determining Volume by Systematic Manual Point Count," ASTM International, PA.
[25] Graham, S. M., 2005, "Evaluation of Welds Exhibiting Large Scatter in Charpy Toughness Using the Reference Temperature," *ASTM Journal of Testing and Evaluation, Vol. 23*, pp. 550-556.
[26] Shome, M., 2007, "Effect of Heat-Input on Austenite Grain Size in the Heat-Affected Zone of HSLA-100 Steel," *Materials Science & Engineering A., Vol. 445-446*, pp. 454-460.
[27] LePera, F. S., 1979, "Improved etching technique for the determination of percent martensite in high-strength dual-phase steels," *Metallography, Vol. 12*, pp. 263-268.
[28] Yang, H. S., and Bhadeshia, H. K. D. H., 2009, "Austenite grain size and the martensite-start temperature," *Scripta Materialia, Vol. 60*, pp. 493-495.
[29] Bhadeshia H. K. D. H., 2013, "About calculating the characteristics of the martensite austenite constituent," *Proceedings, International Seminar on Welding of High Strength Pipeline Steels*, CBMM and The Minerals, Metals and Materials Society, USA, pp. 99-106.
[30] Garcia-Junceda, A., Capdevila, C., Caballero, F. G., and Garcia de Andres, C., 2008, "Dependence of Martensite Start Temperature on Fine Austenite Grain Size," *Scripta Materialia, Vol. 58*, pp. 134-137.
[31] Heinze, C., Pittner, A., Rethmeier, M., and Babu, S. S., 2013, "Dependency of Martensite Start Temperature on Prior Austenite Grain Size and its Influence on Welding-Induced Residual Stresses," *Computational Materials Science, Vol. 69*, pp. 251-260.
[32] Guimaraes, J. R. C., and Rios, P. R., 2010, "Martensite start temperature and the austenite grain-size," *Journal of Materials Science, Vol. 45*, pp. 1074-1077.
[33] Koistinen, D. P., and Marburger R. E., 1959, "A general equation prescribing the extent of the austenite-martensite transformation in pure iron-carbon alloys and plain carbon steels," *Acta Metallurgica, Vol. 7*, pp. 59-60.
[34] Fisher, J. C., Hollomon, J. H., and Turnbull D., 1949, "Kinetics of the Austenite-Martensite Transformation," *Metals Transactions, Vol. 185*, pp. 691-700.
[35] Davis, C. L., and King, J. E., 1993, "Effect of cooling rate on intercritically reheated microstructure and toughness in high strength low alloy steel," *Materials Science and Technology, Vol. 9*, pp. 8-15.
[36] Davis, C. L., and King, J. E., 1994, "Cleavage Initiation in the Intercritically Reheated Coarse-Grained Heat-Affected Zone: Part I. Fractographic Evidence," *Metallurgical and Materials Transactions A., Vol. 25*, pp. 563-573.
[37] Reichert, J. M., Garcin, T., Militzer, M., and Poole, W. J., 2012, "Formation of Martemsite/Austenite (M/A) in X80 Linepipe Steel," *Proceedings, 9th International Pipeline Conference*, Calgary, AB.
[38] Moeinifar, S., Kokabi, A. H., and Maddah Hosseini, H. R., 2010, "Influence of Peak temperature during Simulation and Real Thermal Cycles on Microstructure and Fracture Properties of the Reheated Zones," *Materials Design, Vol. 31*, pp. 2948-2955.
[39] Pokluda, J., and Andera, P., 2010, "Micromechanisms of Fracture and Fatigue in the Multi-Scale Context," XIII, ISBN:978-1-84996-265-0, pp. 293.
[40] Li, Y., and Baker, T. N., 2010, "Effect of Morphology of Martensite-Austenite Phase on Fracture of Weld Heat Affected Zone in Vanadium and Niobium Microalloyed Steels," *Materials Science and Technology, Vol. 26*, pp. 1029-1040.